



ELSEVIER

Contents lists available at ScienceDirect

Journal of Luminescence

journal homepage: [www.elsevier.com/locate/jlumin](http://www.elsevier.com/locate/jlumin)

# Excited-state charge coupled proton transfer reaction in dipole-functionalized salicylideneaniline

Kew-Yu Chen\*, Jiun-Wei Hu

Department of Chemical Engineering, Feng Chia University, 40724 Taichung, Taiwan, ROC

## ARTICLE INFO

### Article history:

Received 25 July 2014

Received in revised form

10 October 2014

Accepted 11 November 2014

Available online 20 November 2014

### Keywords:

ESICT

ESIPT

Salicylideneaniline derivatives

Stokes shift

X-ray diffraction

DFT calculations

## ABSTRACT

Based on design and synthesis of salicylideneaniline derivatives **1–4**, we demonstrate an exceedingly useful system to investigate the excited-state intramolecular charge transfer (ESICT) coupled with excited-state intramolecular proton transfer (ESIPT) reaction via the dipolar functionality of Schiff base salicylideneaniline. In solid and aprotic solvents **1–4** exist mainly as *E* conformers that possess a strong intramolecular six-membered-ring hydrogen bond. Compounds **2–4** exhibit solely a long-wavelength proton-transfer tautomer emission, while dipole-functionalized Schiff base **1** exhibits remarkable dual emission due to the different solvent-polarity environments between ESICT and ESIPT states. Moreover, the geometric structures, frontier molecular orbitals (MOs) and the potential energy curves for **1–4** in the ground and the first singlet excited state were fully rationalized by density functional theory (DFT) and time-dependent DFT calculations.

© 2014 Elsevier B.V. All rights reserved.

## 1. Introduction

Schiff bases [1,2] have been drawing much attention due to their potential application in many areas such as organic dyes [3–5], catalysts [6], liquid crystals [7], and intermediates in organic synthesis [8]. Furthermore, many Schiff bases exhibit a broad range of biological activities [9–11]. For instance, salicylideneaniline (**4**, Scheme 1) derivatives are effective against *Mycobacterium tuberculosis* H37Rv [12]. The excited-state intramolecular proton transfer (ESIPT) reaction [13–16] of salicylideneaniline derivatives, which incorporates transfer of a hydroxyl (amino) proton to the imine nitrogen (carbonyl oxygen) through a pre-existing intramolecular hydrogen bonding configuration, has also been widely reported in the literature [17,18]. As depicted in Fig. 1, the resulting proton-transfer tautomer possesses significant differences in structure and electronic configuration from its corresponding ground state, i.e., a large Stokes shifted  $S_1(K^*) \rightarrow S_0(K)$  fluorescence. This unique optical property has found many important applications, including probes for solvation dynamics [19] and biological environments [20], chemosensors [21–24], photochromic materials [25], and organic light-emitting diodes [26–28]. In Addition, several relevant examples have recently been explored by anchoring the ESIPT molecules with a strong electron-donating group such as dialkylamines, so that upon Franck–Condon excitation,

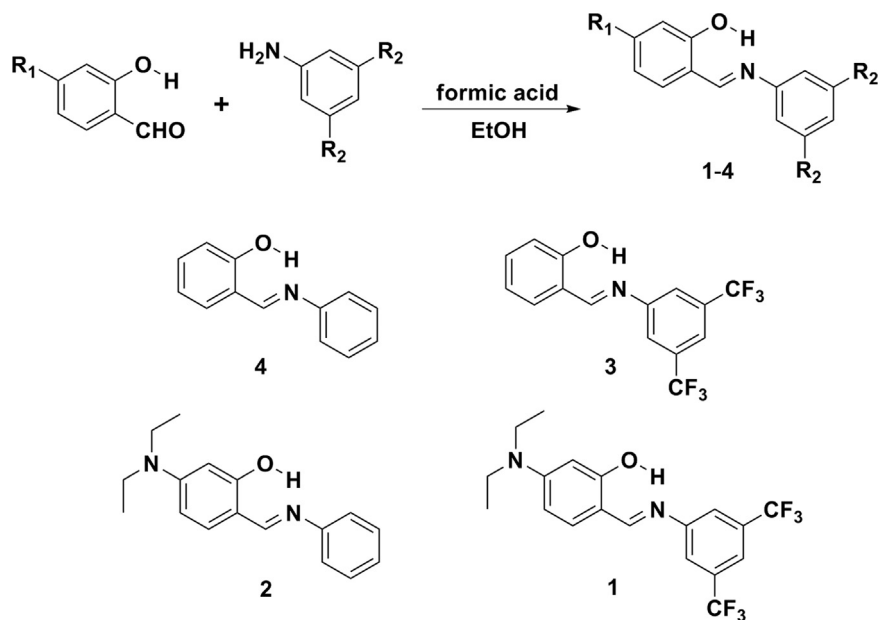
excited-state intramolecular charge transfer (ESICT) may take place. To probe this fundamental issue, studies of the ESICT/ESIPT coupled reaction in *N,N*-dialkylamino-3-hydroxyflavone and 2-hydroxy-4-(di-*p*-tolylamino)benzaldehyde [29] have been performed with femtosecond techniques to investigate the dynamics of the reactions. Based on the chemical design, the research herein reports a practical approach to create the ESICT/ESIPT coupled system via the dipolar functionality of Schiff base X-salicylidene-Y-aniline with X=N(CH<sub>3</sub>)<sub>2</sub> as an electron donor substituent and Y=CF<sub>3</sub> as an electron acceptor substituent.

## 2. Experimental

### 2.1. General

The starting materials such as 2-hydroxybenzaldehyde, 4-(diethylamino)-2-hydroxybenzaldehyde, aniline, 3,5-bis(trifluoromethyl)aniline, formic acid, and ethanol were purchased from Merck, ACROS and Sigma-Aldrich. Solvents were distilled freshly according to a standard procedure. Column chromatography was performed using silica gel Merck Kieselgel Si 60 (40–63 mesh). <sup>1</sup>H NMR spectra were recorded in CDCl<sub>3</sub> on a Bruker 400 MHz NMR spectrometer. Mass spectra were recorded on a VG70-250S mass spectrometer. The absorption and emission spectra were measured using a Jasco V-570 UV–vis spectrophotometer and a Hitachi F-7000 fluorescence spectrophotometer, respectively.

\* Corresponding author. Tel: +886 4 24517250x3683; fax: +886 4 24510890.  
E-mail address: [kyuchen@fcu.edu.tw](mailto:kyuchen@fcu.edu.tw) (K.-Y. Chen).



Scheme 1. The synthetic route and the structures for 1–4.

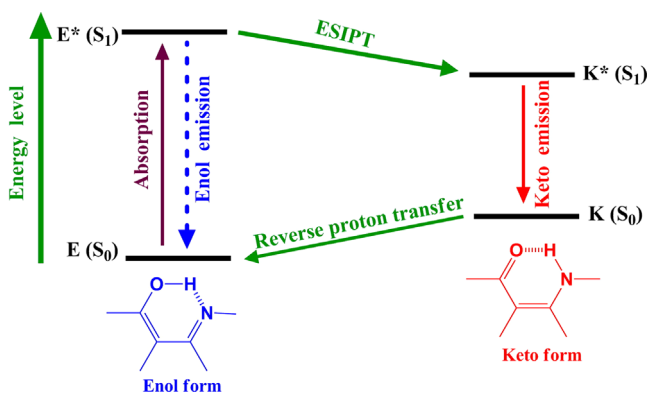


Fig. 1. Characteristic four-level photocycle scheme of the ESIPt process.

## 2.2. Synthesis and characterization

The general procedure for the synthesis of Schiff bases (**1–4**): nonsubstituted/substituted aniline (6.0 mmol) and formic acid (0.1 mL) were added to a mixture of nonsubstituted/substituted 2-hydroxybenzaldehyde (5.2 mmol) and molecular sieves of 4 Å (0.5 g) in ethanol (25 mL) at room temperature. The mixture was refluxed for 10 h. After cooling, the mixture was poured into the cold water and extracted with  $\text{CH}_2\text{Cl}_2$  and dried with anhydrous  $\text{MgSO}_4$ . After solvent was removed, the crude product was purified by silica gel column chromatography with eluent  $\text{CH}_2\text{Cl}_2$  to produce the title compounds (**1–4**) in 85% yield. Characterization data for **1**:  $^1\text{H NMR}$  (400 MHz,  $\text{CDCl}_3$ )  $\delta$  13.00 (br, 1H), 8.44 (s, 1H), 7.66 (s, 1H), 7.62 (s, 2H), 7.21 (d,  $J=8.5$  Hz, 1H), 6.30 (dd,  $J_1=8.5$  Hz,  $J_2=2.0$  Hz, 1H), 6.20 (d,  $J=2.0$  Hz, 1H), 3.42 (q,  $J=7.5$  Hz, 4H), 1.22 (t,  $J=7.0$  Hz, 6H);  $^{13}\text{C NMR}$  (100 MHz,  $\text{CDCl}_3$ )  $\delta$  163.73, 162.91, 152.62, 150.98, 134.56, 132.71, 132.45, 124.33, 122.16, 121.13, 118.34, 104.34, 97.50, 44.68, 12.65; MS (FAB)  $m/z$  (relative intensity) 405 ( $\text{M}+\text{H}^+$ , 100); HRMS calcd. for  $\text{C}_{19}\text{H}_{19}\text{F}_6\text{N}_2\text{O}$  405.1402, found 405.1408. Selected data for **2**:  $^1\text{H NMR}$  (400 MHz,  $\text{CDCl}_3$ )  $\delta$  13.85 (br, 1H), 8.42 (s, 1H), 7.15–7.40 (m, 6H), 6.26 (dd,  $J_1=8.5$  Hz,  $J_2=2.0$  Hz, 1H), 6.19 (s, 1H), 3.42 (q,  $J_1=7.0$  Hz, 4H), 1.23 (t,  $J=7.0$  Hz, 6H);  $^{13}\text{C NMR}$  (100 MHz,  $\text{CDCl}_3$ )  $\delta$  164.27, 160.41, 151.80, 148.77, 133.70, 129.21, 125.42, 120.73, 109.08, 103.72, 97.78, 44.55, 12.67; MS (FAB)  $m/z$  (relative intensity) 269 ( $\text{M}+\text{H}^+$ , 100); HRMS calcd. for  $\text{C}_{17}\text{H}_{21}\text{N}_2\text{O}$  269.1654, found

269.1658. Selected data for **3**:  $^1\text{H NMR}$  (400 MHz,  $\text{CDCl}_3$ )  $\delta$  12.44 (br, 1H), 8.67 (s, 1H), 7.79 (s, 1H), 7.69 (s, 2H), 7.44–7.47 (m, 2H), 7.07 (d,  $J=8.0$  Hz, 2H), 7.00 (t,  $J=8.0$  Hz, 1H); MS (FAB)  $m/z$  (relative intensity) 334 ( $\text{M}+\text{H}^+$ , 100); HRMS calcd. for  $\text{C}_{15}\text{H}_{10}\text{F}_6\text{NO}$  334.0667, found 334.0661. Selected data for **4**:  $^1\text{H NMR}$  (400 MHz,  $\text{CDCl}_3$ )  $\delta$  13.26 (br, 1H), 8.62 (s, 1H), 7.36–7.44 (m, 4H), 7.30–7.25 (m, 3H), 7.04 (d,  $J=8.5$  Hz, 1H), 6.96 (t,  $J=7.5$  Hz, 1H); MS (FAB)  $m/z$  (relative intensity) 198 ( $\text{M}+\text{H}^+$ , 100); HRMS calcd. for  $\text{C}_{13}\text{H}_{12}\text{NO}$  198.0919, found 198.0915.

## 2.3. Crystal structural determination

A single crystal of **3** with dimensions of 0.66 mm  $\times$  0.40 mm  $\times$  0.32 mm was selected. The lattice constants and diffraction intensities were measured with a Bruker Smart 1000 CCD area detector radiation ( $\lambda=0.71073$  Å) at 110(2) K. An  $\omega$ - $2\theta$  scan mode was used for data collection in the range of  $2.95 \leq \theta \leq 29.20^\circ$ . A total of 11,946 reflections were collected and 3340 were independent ( $R_{\text{int}}=0.0283$ ), of which 2572 were considered to be observed with  $I > 2\sigma(I)$  and used in the succeeding refinement. The structure was solved by direct methods with a SHELXS-97 [30] and refined on  $F^2$  by full-matrix least-squares procedure with the Bruker SHELXL-97 packing [31]. All non-hydrogen atoms were refined with anisotropic thermal parameters. The hydrogen atoms refined with riding model position parameters isotropically were located from difference Fourier map and added theoretically. At the final cycle of refinement,  $R=0.0478$  and  $wR=0.1208$  ( $w=1/[\sigma^2(F_o^2)+(0.0653P)^2+0.3824P]$ , where  $P=(F_o^2+2F_c^2)/3$ ).  $S=1.071$ ,  $(\Delta/\sigma)_{\text{max}}=0.001$ ,  $(\Delta/\rho)_{\text{max}}=0.337$  and  $(\Delta/\rho)_{\text{min}}=-0.284$  e/Å<sup>3</sup>.

## 2.4. Computational methods

The Gaussian 03 program was used to perform the ab initio calculation on the molecular structure [32]. Geometry optimizations for compounds **1–4** were carried out with the 6-31G\*\* basis set to the B3LYP functional. The hybrid DFT functional B3LYP has proven to be a suitable DFT functional to describe hydrogen bond [33]. Vibrational frequencies were also performed to check whether the optimized geometrical structures for all compounds were at energy minima, transition states, or higher order saddle points. After obtaining the converged geometries, the TD-B3LYP/6-

Download English Version:

<https://daneshyari.com/en/article/5399623>

Download Persian Version:

<https://daneshyari.com/article/5399623>

[Daneshyari.com](https://daneshyari.com)